$p + d \rightarrow {}^3\mathrm{He} + \gamma$ reaction with pionless effective field theory

H. Nematollahi,* S. Bayegan,† N. Mahboubi,‡ and M. Moeini Arani§
Department of Physics, University of Tehran, P.O. Box 14395-547, Tehran, Iran

(Received 8 May 2016; revised manuscript received 31 August 2016; published 15 November 2016)

We study the proton radiative capture by a deuteron with the pionless effective field theory [EFT($\not\pi$)] formalism. The calculation of the $pd \rightarrow {}^3\mathrm{He}\,\gamma$ amplitude is considered for the incoming doublet and quartet channels leading to the formation of a ^{3}He. The strong and Coulomb scattering amplitudes for the proton-deuteron (pd) scattering are included in this study. In this calculation, the properly normalized ^{3}He wave function has been used at each order. We evaluate both $M1$ and $E1$ transitions in the $pd \rightarrow {}^3\mathrm{He}\,\gamma$ process up to NLO. We calculate the total cross section for the $pd \rightarrow {}^3\mathrm{He}\,\gamma$ process based on the cluster-configuration space and compare it with the experimental data. The cross section results are presented for the incoming proton with the energy $0.5 \leqslant E \leqslant 3$ MeV where the lower and upper limits are chosen for the treatment of Coulomb effects perturbatively and the EFT($\not\pi$) breakdown scale, respectively. No three-body force is needed to renormalize observables up to NLO other than those we have introduced in the pd scattering amplitudes.

DOI: 10.1103/PhysRevC.94.054004

I. INTRODUCTION

The $pd \rightarrow {}^3\mathrm{He}\,\gamma$ reaction performs a prominent role in the evolution of protostars. A reliable knowledge of the physics of protostellar evolution is of fundamental importance [1,2]. The study of astrophysical nucleosynthesis reactions like neutron-deuteron (nd) and proton-deuteron (pd) radiative capture reactions were pioneered at the low energies based on the model-dependent approaches [3,4]. The model-independent and precession controlled pionless effective field theory [EFT($\not\pi$)] approach has successfully been used in the study of $nd \rightarrow {}^3\mathrm{H}\,\gamma$ up to N^{2}LO. The magnetic dipole ($M1$) transition at the very-low-energy regime is a dominant piece in the amplitude of the $nd \rightarrow {}^3\mathrm{H}\,\gamma$ process. The calculation of all $M1$ diagrams have been performed recently for zero energy in the $nd \rightarrow {}^3\mathrm{H}\,\gamma$ reaction [5,6]. The experimental data of the $pd \rightarrow {}^3\mathrm{He}\,\gamma$ reaction in the low-energy regime indicate that the electric dipole ($E1$) transition is dominated, and the $M1$, $E2$ transitions have small contributions [7,8].

In the present study, we apply EFT($\not\pi$) to the low-energy $pd \rightarrow {}^3\mathrm{He}\,\gamma$ process. In this respect, the dominated electromagnetic $E1$ transition is considered using one-body currents up to next-to-leading order (NLO), but the magnetic one- and two-body currents contribute in the $M1$ transition up to NLO. In addition to the strong interaction the Coulomb interaction is also included. The pd scattering is the building block of the $pd \rightarrow {}^3\mathrm{He}\,\gamma$ transition. The pd scattering amplitude is calculated based on the Coulomb proton-proton (pp) scattering [9] and the cluster configuration space constructed by two protons and one neutron [10–12]. In this paper to achieve cut-of independent observables, we have used an analytical approximation form for the leading-order (LO) three-body force (3BF) in the pd scattering. However, at the NLO we use the 3BF which is numerically obtained by fixing the NLO correction to give the correct ^{3}He binding energy. Recently, the analytical form of the NLO 3BF for the pd scattering has been derived and the assessment of the agreement between the analytical form and the numerical fixing of the NLO three-body force has been presented [13].

The formalism and results in this paper are as follows. The electromagnetic (EM), strong and Coulomb interactions are introduced in Sec. II. The pd scattering is introduced in Sec. III. The formalism of $pd \rightarrow {}^3\mathrm{He}\,\gamma$ is presented in Sec. IV, and the numerical results for the pd radiative capture is discussed in Sec. V. Finally we summarize the paper in Sec. VI.

II. INTERACTIONS

The degrees of freedom in the $pd \rightarrow {}^3\mathrm{He}\,\gamma$ process at the low energies are neutron and proton. In this regime, the neutron and proton momentums are as a low-momentum scale Q and the high-momentum parameters are scaled by $\bar{\Lambda} \sim m_\pi$ with m_π as the pion mass.

The interactions of the nucleons in the $pd \rightarrow {}^3\mathrm{He}\,\gamma$ transition can be classified as the strong, Coulomb, and EM sectors. We initially explain briefly about these interactions up to NLO in the following.

A. Strong

We follow the power counting and notations presented in Ref. [5]. We consider the inverse of the scattering lengths of the singlet and triplet nucleon-nucleon (NN) systems, $1/(a_s = -23.714)\,\mathrm{fm}^{-1}$ and $1/(a_t = 4.318)\,\mathrm{fm}^{-1}$, as a low-momentum scale Q, however, the inverse of the effective ranges of the ${}^1S_0$ and ${}^3S_1$ NN states, $1/(\rho_s = 2.73)\ \mathrm{fm}^{-1}$ and $1/(\rho_t = 1.765)\ \mathrm{fm}^{-1}$, are related to the high-momentum scale $\bar{\Lambda}$. The strong interaction for the pd system in the EFT($\not\pi$) formalism using a dibaryon auxiliary field are given by the

*hnematollahi.91@ut.ac.ir
†Corresponding author: bayegan@ut.ac.ir
‡n.mahboubi@ut.ac.ir
§m.moeini.a@ut.ac.ir

S-wave Lagrangian [10,14]

$$\mathcal{L}_s = N^\dagger\left(iD_0+\frac{\vec{D}^2}{2m_N}\right)N + d_s^{A\dagger}\left[\Delta_s - c_{0s}\left(iD_0+\frac{\vec{D}^2}{4m_N}+\frac{\gamma_s^2}{m_N}\right)\right]d_s^A + d_t^{i\dagger}\left[\Delta_t - c_{0t}\left(iD_0+\frac{\vec{D}^2}{4m_N}+\frac{\gamma_t^2}{m_N}\right)\right]d_t^i$$
$$-\left(y_s d_s^{A\dagger}(N^\dagger P^A N) + y_t d_t^{i\dagger}(N^\dagger P^i N) + \text{H.c.}\right) + \frac{m_N H(E,\Lambda)}{6} N^\dagger\big(y_t^2 (d_t^i\sigma_i)^\dagger (d_t^j\sigma_j) - \left[y_t y_s (d_t^i\sigma_i)^\dagger(d_s^A\sigma_A) + \text{H.c.}\right]$$
$$+ y_s^2 (d_s^A\tau_A)^\dagger (d_s^B\sigma_B)\big)N + \cdots, \tag{1}$$

where D_μ is the covariant derivative which acts on the nucleon and dibaryon fields with $\partial_\mu + ie\frac{1+\tau_3}{2}A_\mu$ and $\partial_\mu + ieCA_\mu$ relations, respectively. A_μ and e are the external field and the electron charge. We have $C = 2,1$, and 0 for proton-proton, proton-neutron, and neutron-neutron dibaryons. In Eq. (1), N, d_t^i, and d_s^A denote the nucleon, the deuteron, and the $^1S_0$ NN auxiliary fields, respectively.

The operators

$$P^i = \frac{1}{\sqrt{8}}\sigma_2\sigma^i\tau_2, \qquad P^A = \frac{1}{\sqrt{8}}\sigma_2\tau_2\tau^A \tag{2}$$

with τ_A (σ_i) as isospin (spin) Pauli matrices project the NN system to the $^3S_1$ and $^1S_0$ states, respectively. m_N represents the nucleon mass and the three-nucleon force is introduced by $H(E,\Lambda)$, where E and Λ are the total energy and cutoff momentum. The $H(E,\Lambda)$ which absorbs all dependencies on the cutoff as $\Lambda \to \infty$ is given by [15–17]

$$H(E,\Lambda) = \frac{2}{\Lambda^2}\sum_{m=0}^{\infty} H_{2m}(\Lambda)\left(\frac{m_N E + \gamma_t^2}{\Lambda^2}\right)^m$$
$$= \frac{2H_0(\Lambda)}{\Lambda^2} + \frac{2H_2(\Lambda)}{\Lambda^4}(m_N E + \gamma_t^2) + \cdots, \tag{3}$$

where the interactions proportional to H_{2m} enter at N^{2m}LO [15].

We consider two coupling constants for the singlet and triplet channels as $y_{t,s}^2 = \frac{8\pi}{m_N^2 \rho_{t,s}}$. The parameters $\Delta_{s/t}$ and $c_{0s/t}$ are given by matching the EFT($\not\pi$) NN scattering amplitude to the effective range expansion (ERE) of the scattering amplitude of two nonrelativistic nucleons around the $i\gamma_{s/t}$ [10], and $\gamma_t = 45.702$ MeV is the binding momentum of the deuteron. We note that according to our power counting $\Delta_{s/t} \sim Q$ enters at LO, however, the dimensionless parameter $c_{0s/t} \sim Q^0$ first appears at NLO since it comes with two powers of momentum, $c_{0s/t}p^2 \sim Q^2$. Using the Lagrangian (1), the single nucleon propagator is given by the relation

$$i\Delta_N(E,q) = \frac{i}{E - \frac{q^2}{2m_N} - i\epsilon}, \tag{4}$$

and we obtain the propagators of the triplet and singlet auxiliary fields up to N^{n}LO ($n \leqslant 1$) as

$$D_t^{(n)}(q_0,q) = \frac{4\pi}{m_N y_t^2}\frac{1}{\gamma_t - \sqrt{\frac{q^2}{4} - m_N q_0 - i\varepsilon}} \times \sum_{m=0}^{n}\left(\frac{\frac{\rho_t}{2}\left(m_N q_0 - \frac{q^2}{4} + \gamma_t^2\right)}{\gamma_t - \sqrt{\frac{q^2}{4} - m_N q_0 - i\varepsilon}}\right)^m,$$

$$D_s^{(n)}(q_0,q) = \frac{4\pi}{m_N y_s^2}\frac{1}{\gamma_s - \sqrt{\frac{q^2}{4} - m_N q_0 - i\varepsilon}} \times \sum_{m=0}^{n}\left(\frac{\frac{\rho_s}{2}\left(m_N q_0 - \frac{q^2}{4}\right)}{\gamma_s - \sqrt{\frac{q^2}{4} - m_N q_0 - i\varepsilon}}\right)^m. \tag{5}$$

B. Coulomb

In the pd system, the Coulomb interaction is dominated at the low-momentum regime. As noted in [11,12,18,19], the Coulomb parameter enters as $\frac{\alpha m_N}{p}$, where p is the momentum transfer. With respect to the Coulomb potential

$$V_c = \frac{\alpha}{p^2}, \tag{6}$$

one cannot assume that the scale of all momenta is set by the deuteron binding momentum, γ_t. As it is mentioned in [18], we have to introduce a new momentum scale p, where $p \ll Q$ for the power counting. Thus, we have to make a simultaneous expansion in two small parameters $\frac{Q}{\Lambda}$ and $\frac{p}{\alpha m_N}$.

The Lagrangian of the kinetic and gauge fixing terms of the photons is

$$\mathcal{L}_{ph} = -\frac{1}{4}F_{\mu\nu}F^{\mu\nu} - \frac{1}{2\xi}(\partial_\mu A^\mu - \eta_\mu\eta_\nu\partial^\nu A_\mu)^2,$$
$$\eta_\mu = \text{timelike unit vector}. \tag{7}$$

Therefore the static photon propagator is

$$i\Delta_{ph}(p) = \frac{i}{p^2+\lambda^2}, \tag{8}$$

where λ is the mass of the photon. We consider the mass for the photon because the infrared divergences of the photon propagator should be handled. The final results are obtained using an extrapolation for the $\lambda \to 0$.

By ignoring the Coulomb effects we have two different isospin-symmetric NN states with respect to their spins: singlet and triplet channels. But the pp part of the singlet NN channel has an additional Coulomb contribution. So, the Coulomb interaction makes isospin breaking. The propagator of the pp part of the $^1S_0$ dibaryon at N^{n}LO ($n \leqslant 1$) is given by [13]

$$D_{s,pp}^{(n)}(q_0,q) = \frac{4\pi}{m_N y_s^2}\frac{1}{\frac{1}{a_c} + 2\kappa H\left(\frac{\kappa}{q'}\right)} \times \sum_{m=0}^{n}\left(\frac{\frac{r_c}{2}\left(m_N q_0 - \frac{q^2}{4}\right)}{\frac{1}{a_c} + 2\kappa H\left(\frac{\kappa}{q'}\right)}\right)^m \tag{9}$$

with

$$\alpha = \frac{e^2}{4\pi} \sim \frac{1}{137}, \quad \kappa = \frac{\alpha m_N}{2}, \quad q' = i\sqrt{\frac{q^2}{4} - m_N q_0 - i\epsilon}, \tag{10}$$

and

$$H(\eta) = \psi(i\eta) + \frac{1}{2i\eta} - \log(i\eta). \tag{11}$$

In Eq. (11) the function ψ denotes the logarithmic derivative of the Γ function. Also, the scattering length and effective range for the pp channel are introduced by $a_c = -7.806$ fm and $r_c = 2.794$ fm, respectively.

C. Electromagnetic

The $E1$, $M1$, and $E2$ transitions contribute to the $pd \to {}^3\mathrm{He}\,\gamma$ amplitude at the low-energy regime. With respect to the experimental facts for the $pd \to {}^3\mathrm{He}\,\gamma$ reaction, the contribution of the $E2$ transition is small in comparison with the $M1$ transition at low energy. We therefore evaluate the contributions of $E1$ and $M1$ transitions in this calculation.

The Lagrangian of the $E1$ one-body current is given by the minimal substitution of $\vec{\nabla} \to \vec{\nabla} + ie\frac{(1+\tau_3)}{2}\vec{A}$ in the Lagrangian of Eq. (1) with $\vec{A}$ as an external field:

$$\mathcal{L}_E = \frac{e}{2m_N} N^\dagger \left(\frac{1+\tau_3}{2}\right)(\vec{P} + \vec{P}') \cdot \vec{\varepsilon}^{*}{}_{\gamma} N, \tag{12}$$

where $\vec{P}$ and $\vec{P}'$ are momenta for the incoming and outgoing nucleons and $\vec{\varepsilon}_\gamma$ denotes the three-vector polarization of the produced photon. We note that the contribution of the $E1$ two-body current enters first at higher order than NLO [20]. The Lagrangian of the $M1$ interaction is constructed by considering the nucleon and dibaryon operators coupling to the magnetic field $\vec{B}$,

$$\mathcal{L}_B = \frac{e}{2m_N} N^\dagger (k_0 + k_1\tau^3)\vec{\sigma}\,\vec{B} N + \frac{eL_1}{m_N\sqrt{\rho_t\rho_s}} d_t^{j\dagger} d_s^3 B_j - \frac{2eL_2}{m_N\rho_t} i\varepsilon_{ijk} d_t^{i\dagger} d_t^j B_k + \mathrm{H.c.}, \tag{13}$$

where $k_0 = \frac{1}{2}(k_p + k_n) = 0.4399$ and $k_1 = \frac{1}{2}(k_p - k_n) = 2.35294$. k_p (k_n) denotes the proton (neutron) magnetic moment. The coefficients $L_1 = -4.427 \pm 0.015$ fm and $L_2 = -0.4$ fm which have been fixed using the cross section of $np \to d\gamma$ at thermal energy, and the deuteron magnetic moment μ_M, enter at NLO [21].

III. *pd* SCATTERING

In this section, we explain about a major building block of the $pd \to {}^3\mathrm{He}\,\gamma$ transition, the pd scattering. As was investigated in [12], nucleon-dibaryon scattering amplitudes up to NLO constructed by two protons and one neutron are evaluated using the diagrams which are shown in Fig. 1.

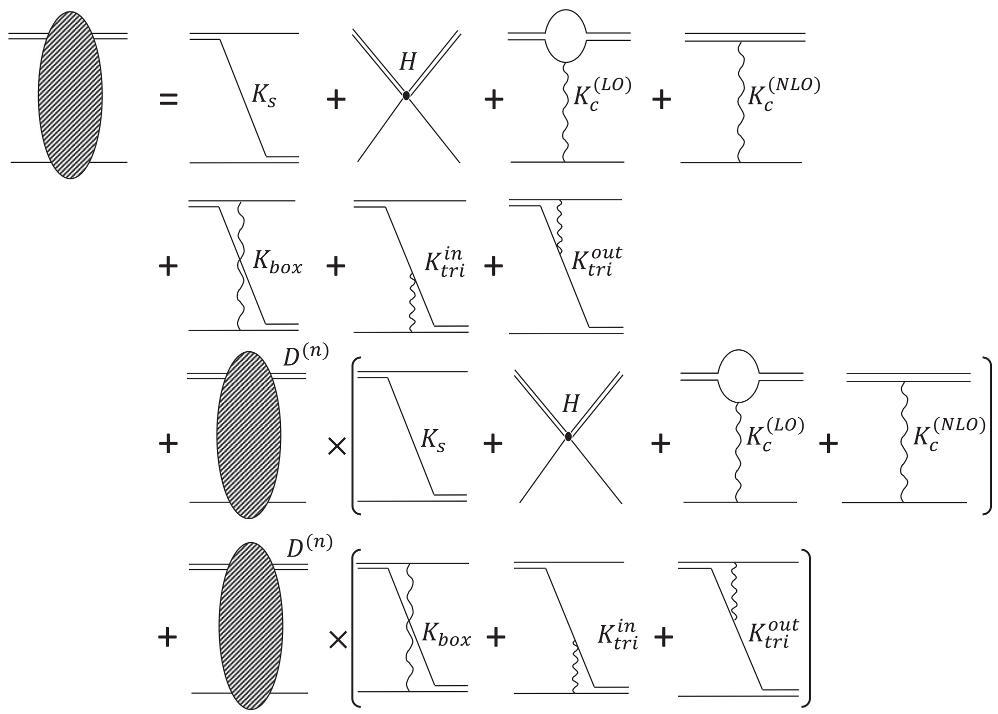

FIG. 1. The Faddeev equation of the nucleon-dibaryon scattering in the cluster-configuration space up to the next-to-leading order. The superscript "n" denotes the contribution up to N^{n}LO ($n \leqslant 1$). The dashed oval is the nucleon-dibaryon scattering amplitude. The solid line indicates a nucleon. The Coulomb internal wavy line with coupling to nucleon from both sides represents an exchanged photon. The double solid line denotes a dibaryon auxiliary field with the propagator $\mathcal{D}^{(n)}$. The K_s and H depict the propagator of the exchanged nucleon and the three-body force, respectively. The K_c, K_{box}, $K_{\mathrm{tri}}^{\mathrm{in}}$, and $K_{\mathrm{tri}}^{\mathrm{out}}$ denote the kernels with the Coulomb interaction $\sim\alpha$. The diagram with direct Coulomb between the nucleon and deuteron enters only at the next-to-leading order.

In Fig. 1, all diagrams $\sim\mathcal{O}(\alpha)$ are shown in the cluster-configuration space. We do not consider diagrams of the second and fourth lines for calculating the Coulomb contributions, because they have a small contribution in the final results ($K_{\rm box}$ has a 7% effect, also $K_{\rm tri}^{\rm in}$ and $K_{\rm tri}^{\rm out}$ have 15% contribution compared to the simple nucleon-exchanged diagram without the photon [12]). The dashed oval represents the nucleon-dibaryon scattering amplitude with the Coulomb effect. In the cluster-configuration space the N^{n}LO($n \leqslant 1$) dibaryon propagators are given by

$$\mathcal{D}^{(n)}(q_0,q) = \begin{pmatrix} D_t^{(n)}\big(q_0 - \frac{q^2}{2m_N},q\big) & 0 & 0 \\ 0 & D_s^{(n)}\big(q_0 - \frac{q^2}{2m_N},q\big) & 0 \\ 0 & 0 & D_{s,pp}^{(n)}\big(q_0 - \frac{q^2}{2m_N},q\big) \end{pmatrix}. \tag{14}$$

We note that the diagram with the direct coupling of the photon to the dibaryon enters first at NLO, so we do not consider it at the LO calculations.

The quartet nucleon-dibaryon scattering amplitude has been made only by the scattering from the incoming $N + d_t$ to the outgoing $N + d_t$ channel. By using the projection operators for S and P waves one can project the nucleon-dibaryon system to the ${}^4S_{\frac{3}{2}}$, ${}^4P_{\frac{1}{2}}$, and ${}^4P_{\frac{3}{2}}$ channels [22]. Therefore, in the cluster-configuration space, the Faddeev equation of the diagrams in Fig. 1 for the quartet channel has only the nonzero component $t_{q,\,t\to t}^{(n,L)}$ which represents the amplitude in the quartet channel for the $d_t\, p \to d_t\, p$ transition,

$$\begin{aligned} t_{q,\,t\to t}^{(n,L)}(E;k,p) &= -m_N y_t^2\bigg[K_{s,L}(E;k,p) - \frac{1}{2}K_{c,L}^{(t),n}(E;k,p)\bigg] + \frac{m_N y_t^2}{2\pi^2}\int_0^\Lambda dq\, q^2\bigg[K_{s,L}(E;q,p) - \frac{1}{2}K_{c,L}^{(t),n}(E;q,p)\bigg] \\ &\quad \times D_t^{(n)}\bigg(E - \frac{q^2}{2m_N},q\bigg)\, t_{q,\,t\to t}^{(n,L)}(E;k,q). \end{aligned} \tag{15}$$

Thus the 3×1 quartet amplitude for the pd scattering is given by

$$t_q^{(n,L)}(E;k,p) \equiv \begin{pmatrix} t_{q,\,t\to t}^{(n,L)} \\ 0 \\ 0 \end{pmatrix}(E;k,p), \tag{16}$$

where $E = \frac{3k^2}{4m_N} - \frac{\gamma_t^2}{m_N}$, k and p are the total center of mass (c.m.) energy of the nucleon-dibaryon system, the incoming, and outgoing momentums, respectively. In Eq. (15), the propagator of the exchanged nucleon, $K_{s,L}$, is given by

$$K_{s,L}(E;k,p) = \frac{1}{2}\int_{-1}^{1} d(\cos\theta)\frac{P_L(\cos\theta)}{k^2 + p^2 - m_N E + kp\cos\theta}, \tag{17}$$

where $P_L(x)$ denotes the Lth Legendre polynomial of the first kind and θ indicates the angle between $\vec{k}$ and $\vec{p}$ vectors. The $K_{c,L}^{(t,s),n}$ kernels which are the contributions of the third and fourth diagrams of lines 1 and 3 in Fig. 1 are obtained with the relations

$$K_{c,L}^{(t,s),n}(E;k,p) = \frac{\alpha m_N}{2kp}Q_L\bigg(-\frac{k^2 + p^2 + \lambda^2}{2kp}\bigg)\bigg(\frac{1}{|\gamma_t|} - \delta_{n1}\rho_{t,s}\bigg), \qquad n = 0,1. \tag{18}$$

For the doublet (${}^2S_{\frac{1}{2}}$, ${}^2P_{\frac{1}{2}}$, and ${}^2P_{\frac{3}{2}}$) channels, the nucleon-dibaryon scattering amplitudes in the cluster-configuration space constructed by two protons and one neutron are given by

$$\begin{aligned} \begin{pmatrix} t_{d,\,t\to t}^{(n,L)} \\ t_{d,\,t\to s_1}^{(n,L)} \\ t_{d,\,t\to s_2}^{(n,L)} \end{pmatrix} &= \frac{m_N}{2}\begin{pmatrix} y_t^2(K_{s,L} + \delta_{L0}H(E,\Lambda)) \\ -y_t y_s\big(K_{s,L} + \delta_{L0}\frac{H(E,\Lambda)}{3}\big) \\ -y_t y_s\big(2K_{s,L} + \delta_{L0}\frac{2H(E,\Lambda)}{3}\big) \end{pmatrix} + \frac{m_N}{2}\begin{pmatrix} y_t^2 K_{c,L}^{(t),n} \\ 0 \\ 0 \end{pmatrix} \\ &\quad - \frac{m_N}{2}\begin{pmatrix} y_t^2 D_t^{(n)}(K_{s,L} + \delta_{L0}H(E,\Lambda)) & -y_t y_s D_s^{(n)}(3K_{s,L} + \delta_{L0}H(E,\Lambda)) & 0 \\ -y_t y_s D_t^{(n)}\big(K_{s,L} + \delta_{L0}\frac{H(E,\Lambda)}{3}\big) & -y_s^2 D_s^{(n)}\big(K_{s,L} - \delta_{L0}\frac{H(E,\Lambda)}{3}\big) & 0 \\ -y_t y_s D_t^{(n)}\big(2K_{s,L} + \delta_{L0}\frac{2H(E,\Lambda)}{3}\big) & y_s^2 D_s^{(n)}\big(2K_{s,L} + \delta_{L0}\frac{2H(E,\Lambda)}{3}\big) & 0 \end{pmatrix} \otimes \begin{pmatrix} t_{d,\,t\to t}^{(n,L)} \\ t_{d,\,t\to s_1}^{(n,L)} \\ t_{d,\,t\to s_2}^{(n,L)} \end{pmatrix} \\ &\quad - \frac{m_N}{2}\begin{pmatrix} y_t^2 D_t^{(n)} K_{c,L}^{(t),n} & 0 & -y_t y_s D_{s,pp}^{(n)}(3K_{s,L} + \delta_{L0}H(E,\Lambda)) \\ 0 & y_s^2 D_s^{(n)} K_{c,L}^{(s),n} & y_s^2 D_{s,pp}^{(n)}\big(K_{s,L} + \delta_{L0}\frac{H(E,\Lambda)}{3}\big) \\ 0 & 0 & \delta_{L0} y_s^2 D_{s,pp}^{(n)}\frac{2H(E,\Lambda)}{3} \end{pmatrix} \otimes \begin{pmatrix} t_{d,\,t\to t}^{(n,L)} \\ t_{d,\,t\to s_1}^{(n,L)} \\ t_{d,\,t\to s_2}^{(n,L)} \end{pmatrix} \end{aligned} \tag{19}$$

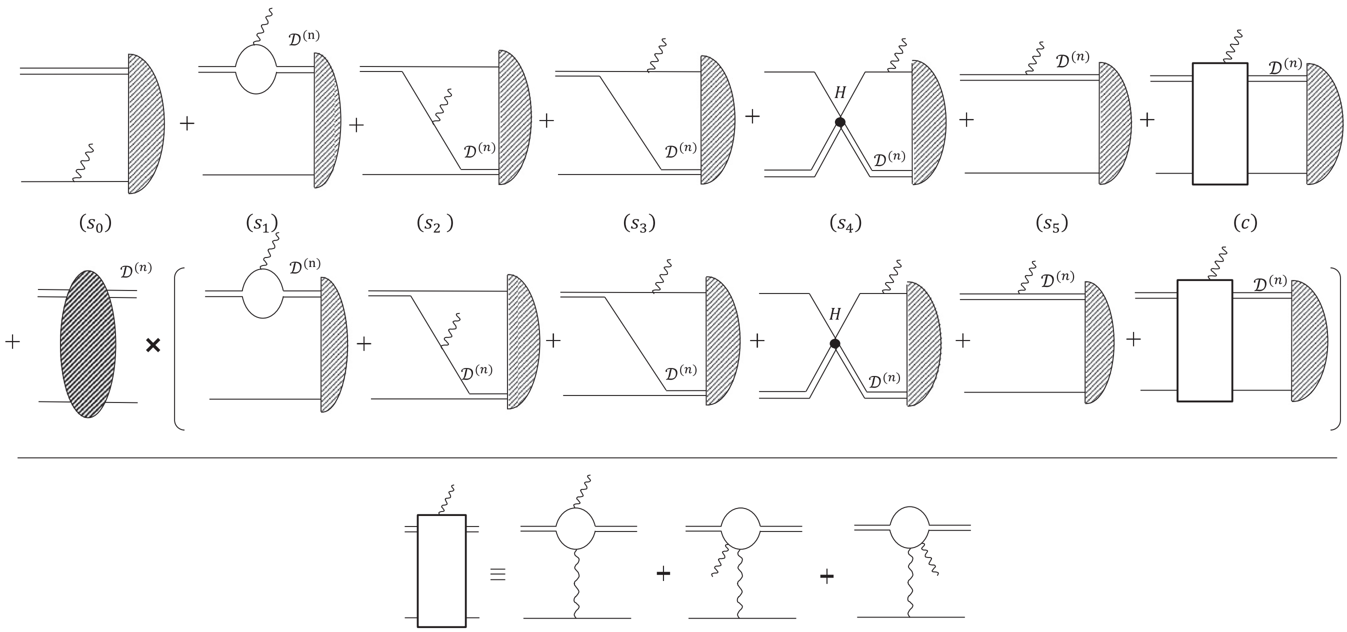

FIG. 2. The Feynman diagrams which contribute in the $E1$ and $M1$ $pd \to {}^3\text{He}\,\gamma$ transition amplitudes up to NLO. The first and second lines show the diagrams which contribute in the $M1$ and $E1$ transitions of the $pd \to {}^3\text{He}\,\gamma$ process up to NLO. For the $E1$ we do not calculate s_5 and the fifth diagram in the second line that are related to the s_5 diagram, because it will appear in a higher order than NLO. The third line presents the diagrams which enter only for the $pd \to {}^3\text{He}\,\gamma$ transition (Coulomb effect). They are depicted by the rectangle with an outgoing wavy line. The wavy line which exits from the nucleon denotes the emitted photon. The dashed half-oval is the normalized ^{3}He wave function. All remaining notations are the same as in Fig. 1.

with

$$A \otimes B \equiv \frac{1}{2\pi^2} \int_0^\Lambda dq\, q^2 A(\ldots q) B(\ldots q). \tag{20}$$

In the above equation, $t^{(n,L)}_{d,\, v \to w}$ denotes the N^{n}LO $d_v N \to d_w N$ transition amplitude in the doublet channel where L denotes the L wave, and v and w are t, s_1, and s_2 for the ${}^3S_1$, ${}^1S_0$, and pp part of ${}^1S_0$ dibaryons, respectively. Here, the single nucleon in the nucleon-dibaryon system is proton, proton, and neutron when the dibaryon is the ${}^3S_1$, ${}^1S_0$, and pp part of ${}^1S_0$, respectively. We emphasize that the relation (19) is constructed by considering the projection operators for the doublet channels [22].

The nucleon-dibaryon scattering amplitudes in Eqs. (15) and (19) enable us to evaluate the amplitude of the $pd \to^3$ He γ transition in the following section by the cluster-configuration space up to NLO.

IV. $pd \to {}^3\text{He}\,\gamma$ SYSTEM

We concentrate on the energy regime $E \geqslant 0.5$ MeV and try to calculate the amplitude of the proton radiative capture by deuteron in the c.m. framework. We work in the region $E \geqslant 0.5$ MeV because in this regime the Coulomb parameter $\frac{\alpha m_N}{p}$ is of order $\frac{1}{3}$ and so, nonperturbative treatment of Coulomb effects is not necessary.

In the absence of the Coulomb repulsion the $pd \to {}^3\text{He}\ \gamma$ process is acting like the $nd \to {}^3\text{He}\ \gamma$ process and the $M1$ transition has the dominated contribution with respect to $E1$ at zero energy. With the presence of the Coulomb repulsion, both the $E1$ and $M1$ transitions amplitudes are small at zero energy. With increasing energy, the amplitude of the $E1$ transition, due to the capture in the P-wave state, increases and contributes dominantly in the $pd \to {}^3\text{He}\ \gamma$ process.

The diagrams of the $E1$ and $M1$ transitions for the $pd \to {}^3\text{He}\ \gamma$ process up to next-to-leading order are schematically shown in Fig. 2. The dashed oval depicts the nucleon-dibaryon scatterings which are given by Eqs. (16) and (19) as the quartet and doublet amplitudes, respectively. The dashed half-oval indicates the normalized ^{3}He wave function at N^{n}LO which is introduced by $t^{(n)}_{{}^3\text{He}}$ in the next section. We consider the contribution of all diagrams shown in Fig. 2 in the amplitude of proton radiative capture by a deuteron reaction. We do not consider the contributions of the diagrams similar to Fig. 3. As noted in [11] these diagrams have negligible contributions in the final results. In the following we calculate the $M1$ and $E1$ amplitude for the $pd \to\ {}^3\text{He}\ \gamma$ process separately.

A. $M1$ transition

By working in the Coulomb gauge, the $M1$ amplitude of the $pd \to^3$ He γ can be written as two orthogonal terms

$$(t^\dagger \sigma_a N)(\vec{\varepsilon}_d \times (\vec{\varepsilon}^*{}_\gamma \times \vec{\hat{q}}))_a\,, \qquad i(t^\dagger N)(\vec{\varepsilon}_d \cdot \vec{\varepsilon}^*{}_\gamma \times \vec{\hat{q}}), \tag{21}$$

where t, $\vec{\varepsilon}_d$, and $\vec{\hat{q}}$ are the final ^{3}He field, the three-vector polarization of the deuteron and the unit vector along the three-momentum of the outgoing photon, respectively.

Using the $M1$ transition, the final ^{3}He ground state can be made from both initial doublet (${}^2S_{\frac{1}{2}}$) and quartet (${}^4S_{\frac{3}{2}}$) pd

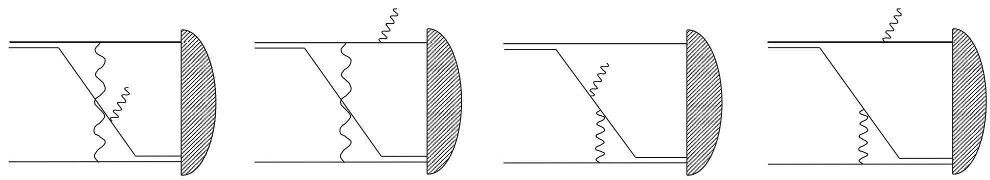

FIG. 3. The neglected diagrams which can be contributed in the final amplitude of the $E1$ and $M1$ $pd \to {}^3\mathrm{He}\,\gamma$ transition. All notations are the same as previous figures.

systems. We calculate the contribution of the diagrams in Fig. 2 step by step as presented for the amplitude of the $nd \to {}^3\mathrm{H}\,\gamma$ reaction in [5]. Thus, the amplitude of the $M1$ $pd \to {}^3\mathrm{He}$ γ transition can generally be written as the sum of both initial ${}^2S_{\frac{1}{2}}$ and ${}^4S_{\frac{3}{2}}$ pd contributions by the relation

$$\mathcal{W}^{(n)}_{M1} = t^{\dagger}\Big[\mathcal{M}^{(n)}_{{}^2S_{\frac{1}{2}}} X_{{}^2S_{\frac{1}{2}}} + \mathcal{M}^{(n)}_{{}^4S_{\frac{3}{2}}} X_{{}^4S_{\frac{3}{2}}}\Big]N, \tag{22}$$

where

$$\begin{aligned} X_{{}^2S_{\frac{1}{2}}} &= i\vec{\varepsilon}_d\vec{\varepsilon}^*{}_{\gamma} \times \vec{q} + \vec{\sigma} \times \vec{\varepsilon}_d\vec{\varepsilon}^*{}_{\gamma} \times \vec{q}\,,\\ X_{{}^4S_{\frac{3}{2}}} &= 2\,i\vec{\varepsilon}_d\vec{\varepsilon}^*{}_{\gamma} \times \vec{q} - \vec{\sigma} \times \vec{\varepsilon}_d\vec{\varepsilon}^*{}_{\gamma} \times \vec{q}\,. \end{aligned} \tag{23}$$

The $\mathcal{M}^{(n)}_x$ with $x = {}^2S_{\frac{1}{2}},\ {}^4S_{\frac{3}{2}}$ for the quartet and doublet channels before multiplying the deuteron wave function normalization factor is given by

$$\begin{aligned} M^{(n)}_x(E_i,k) &= \big[S^{(n)}_{0,x}(E_i,k) + S^{(n)}_x(E_i,k) + C^{(n)}_x(E_i,k)\big]u \\ &\quad - \frac{1}{2\pi^2}\int_0^{\Lambda} dq\, q^2\, \big[S^{(n)}_x(E_i,q) + C^{(n)}_x(E_i,q)\big]\mathcal{D}^{(n)}(E_i,q)\, t^{(n,0)}_x(E_i;k,q) \end{aligned} \tag{24}$$

with

$$S^{(n)}_x(E_i,k) = \sum_{i=1}^{5} S^{(n)}_{i,x}(E_i,k), \qquad u = \begin{pmatrix}1\\0\\0\end{pmatrix}, \tag{25}$$

where the 3×3 matrix function $S^{(n)}_{i,x}$ with $i = 0,\ldots,5$ represents the contribution of the "s_i" diagram in Fig. 2 for the incoming x channel at N^{n}LO ($n \leqslant 1$). In Eq. (24), the matrix function $C^{(n)}_x$ denotes the contribution of the diagram "c" in Fig. 2. The "c" diagram represents the additional terms which only contribute in the $pd \to {}^3\mathrm{He}\,\gamma$ process compare with the $nd \to {}^3\mathrm{H}\,\gamma$. Also, the k indicates the incoming momentum and $E_i = E = \frac{3k^2}{4m_N} - \frac{\gamma_t^2}{m_N}$ denotes the energy of the initial pd system in the c.m. framework.

For the initial ${}^2S_{\frac{1}{2}}$ state, in the cluster-configuration space, we obtain

$$S^{(n)}_{0,{}^2S_{\frac{1}{2}}}(E_i,k) = \frac{e}{6m_N}\frac{1}{E_f - E_i}\, t^{(n)\dagger}_{{}^3\mathrm{He}}(k)\begin{pmatrix} -(k_0+k_1) & 0 & 0\\ 0 & k_0+k_1 & 0\\ 0 & 0 & 2(k_0-k_1)\end{pmatrix},$$

$$S^{(n)}_{1,{}^2S_{\frac{1}{2}}}(E_i,k) = \frac{e\,y_t^2}{48\pi}\frac{1}{E_f - E_i}\, t^{(n)\dagger}_{{}^3\mathrm{He}}(k)\mathcal{D}^{(n)}(E_f,k)\left[\sqrt{\frac{3}{4}k^2 - m_N E_i} - \sqrt{\frac{3}{4}k^2 - m_N E_f}\right]\begin{pmatrix} 2k_0 & k_1 & 0\\ k_1 & 0 & 0\\ 0 & 0 & 0\end{pmatrix},$$

$$\begin{aligned} S^{(n)}_{2,{}^2S_{\frac{1}{2}}}(E_i,k) &= \frac{e\,y_t^2}{96\pi^2}\frac{1}{E_f - E_i}\int_0^{\Lambda} dq\, q^2 t^{(n)\dagger}_{{}^3\mathrm{He}}(q)\mathcal{D}^{(n)}(E_f,q)\frac{1}{kq}\left[Q_0\left(\frac{m_N E_i - k^2 - q^2}{kq}\right) - Q_0\left(\frac{m_N E_f - k^2 - q^2}{kq}\right)\right]\\ &\quad\times\begin{pmatrix} -5(k_0-k_1) & k_0-k_1 & 2(k_0+k_1)\\ k_0-k_1 & -(k_0-k_1) & 2(k_0+k_1)\\ 2(k_0+k_1) & 2(k_0+k_1) & 0\end{pmatrix}, \end{aligned}$$

$$\begin{aligned} S^{(n)}_{3,{}^2S_{\frac{1}{2}}}(E_i,k) &= \frac{e\,y_t^2}{96\pi^2}\frac{1}{E_f - E_i}\int_0^{\Lambda} dq\, q^2\, t^{(n)\dagger}_{{}^3\mathrm{He}}(q)\frac{1}{kq}\left[\mathcal{D}^{(n)}(E_i,q)Q_0\left(\frac{m_N E_i - k^2 - q^2}{kq}\right) - \mathcal{D}^{(n)}(E_f,q)Q_0\left(\frac{m_N E_f - k^2 - q^2}{kq}\right)\right]\\ &\quad\times\begin{pmatrix} k_0+k_1 & -(k_0+k_1) & -2(k_0+k_1)\\ 3(k_0+k_1) & k_0+k_1 & -2(k_0+k_1)\\ 6(k_0-k_1) & -2(k_0-k_1) & 0\end{pmatrix}, \end{aligned}$$

$$S^{(n)}_{4,{}^2S_{\frac{1}{2}}}(E_i,k) = \frac{e\,y_t^2}{72\pi^2}\frac{1}{E_f-E_i}\,H(E_i,\Lambda)\int_0^\Lambda dq\,q^2\,t^{(n)\dagger}_{{}^3\mathrm{He}}(q)[\mathcal{D}^{(n)}(E_f,q)-\mathcal{D}^{(n)}(E_i,q)]\begin{pmatrix}-3(k_0+k_1) & k_0+k_1 & 2(k_0+k_1)\\ -3(k_0+k_1) & (k_0+k_1) & 2(k_0+k_1)\\ -6(k_0-k_1) & 2(k_0-k_1) & 4(k_0-k_1)\end{pmatrix},$$

$$S^{(n)}_{5,{}^2S_{\frac{1}{2}}}(E_i,k) = t^{(n)\dagger}_{{}^3\mathrm{He}}(k)\mathcal{D}^{(n)}(E_f,k)\begin{pmatrix}\frac{-4eL_2}{3m_N\rho_t} & \frac{eL_1}{3m_N\sqrt{\rho_s\rho_t}} & 0\\ \frac{eL_1}{3m_N\sqrt{\rho_s\rho_t}} & 0 & 0\\ 0 & 0 & 0\end{pmatrix},$$

$$C^{(n)}_{{}^2S_{\frac{1}{2}}}(E_i,k) = \frac{e^3y_t^2m_N}{192(\pi)^4}\frac{1}{(E_f-E_i)}\int_0^\Lambda dq'q'^2\int_0^\Lambda dq\,q^2\int_{-1}^1 d(\cos\theta)\,t^{(n)\dagger}_{{}^3\mathrm{He}}(q')\,\mathcal{D}^{(n)}(E_f,q')$$
$$\times\left[\frac{O(E_i,k,q,q',\cos\theta)}{m_NE_i-k^2-q^2-kq\cos\theta}-\frac{O(E_f,k,q,q',\cos\theta)}{m_NE_f-k^2-q^2-kq\cos\theta}\right]\begin{pmatrix}2k_0 & k_1 & 0\\ k_1 & 0 & 0\\ 0 & 0 & 0\end{pmatrix}, \tag{26}$$

where

$$O(E,k,q,q',\cos\theta) = \frac{1}{\sqrt{F}}\left[\ln\left(\frac{A+B}{A-B}\right)-\ln\left(\frac{x1}{x2}\right)\right] \tag{27}$$

with the following parameters:

$$\begin{aligned}&x1 = B(2C+D)-A(D+2G)+2\sqrt{F}\sqrt{C+D+G},\quad x2 = B(2C-D)-A(D-2G)+2\sqrt{F}\sqrt{C-D+G},\\ &A = k^2+q'^2+\lambda^2,\qquad B=-2kq',\quad C=(m_N\,E-k^2-q^2-q'^2-2kq\cos\theta)^2-(qq'\sin\theta)^2,\\ &D = 2(m_N\,E-k^2-q^2-q'^2-2kq\cos\theta)(kq'+qq'\cos\theta),\quad G=(kq'+qq'\cos\theta)^2+(qq'\sin\theta)^2,\\ &F = B^2C+A^2G-ABD.\end{aligned} \tag{28}$$

Also, for the quartet channel (${}^4S_{\frac{3}{2}}$) the amplitudes of the s_0,..., s_5 and c diagrams in Fig. 2 are given by

$$S^{(n)}_{0,{}^4S_{\frac{3}{2}}}(E_i,k) = \frac{e}{3\sqrt{3}m_N}\frac{1}{E_f-E_i}\,t^{(n)\dagger}_{{}^3\mathrm{He}}(k)\begin{pmatrix}k_0+k_1 & 0 & 0\\ 0 & 0 & 0\\ 0 & 0 & 0\end{pmatrix},$$

$$S^{(n)}_{1,{}^4S_{\frac{3}{2}}}(E_i,k) = \frac{e\,y_ty_s}{48\sqrt{3}\pi}\frac{1}{E_f-E_i}\,t^{(n)\dagger}_{{}^3\mathrm{He}}(k)\mathcal{D}^{(n)}(E_f,k)\left[\sqrt{\frac{3}{4}k^2-m_NE_i}-\sqrt{\frac{3}{4}k^2-m_NE_f}\right]\begin{pmatrix}-k_0 & 0 & 0\\ k_1 & 0 & 0\\ 0 & 0 & 0\end{pmatrix},$$

$$S^{(n)}_{2,{}^4S_{\frac{3}{2}}}(E_i,k) = \frac{e\,y_ty_s}{48\sqrt{3}\pi^2}\frac{1}{E_f-E_i}\int_0^\Lambda dqq^2t^{(n)\dagger}_{{}^3\mathrm{He}}(q)\mathcal{D}^{(n)}(E_f,q)$$
$$\times\frac{1}{kq}\left[Q_0\left(\frac{m_NE_i-k^2-q^2}{kq}\right)-Q_0\left(\frac{m_NE_f-k^2-q^2}{kq}\right)\right]\begin{pmatrix}k_0-k_1 & 0 & 0\\ k_0-k_1 & 0 & 0\\ 2(k_0+k_1) & 0 & 0\end{pmatrix},$$

$$S^{(n)}_{3,{}^4S_{\frac{3}{2}}}(E_i,k) = \frac{e\,y_ty_s}{24\sqrt{3}\pi^2}\frac{1}{E_f-E_i}\int_0^\Lambda dqq^2t^{(n)\dagger}_{{}^3\mathrm{He}}(q)\frac{1}{kq}\left[\mathcal{D}^{(n)}(E_i,q)Q_0\left(\frac{m_NE_i-k^2-q^2}{kq}\right)\right.$$
$$\left.-\,\mathcal{D}^{(n)}(E_f,q)Q_0\left(\frac{m_NE_f-k^2-q^2}{kq}\right)\right]\begin{pmatrix}k_0+k_1 & 0 & 0\\ 0 & 0 & 0\\ 0 & 0 & 0\end{pmatrix},\quad S^{(n)}_{4,{}^4S_{\frac{3}{2}}}(E_i,k)=0,$$

$$S^{(n)}_{5,{}^4S_{\frac{3}{2}}}(E_i,k) = t^{(n)\dagger}_{{}^3He}(k)\mathcal{D}^{(n)}(E_f,k)\begin{pmatrix}\frac{2eL_2}{3\sqrt{3}m_N\rho_t} & 0 & 0\\ \frac{eL_1}{3\sqrt{3}m_N\sqrt{\rho_s\rho_t}} & 0 & 0\\ 0 & 0 & 0\end{pmatrix},$$

$$C^{(n)}_{{}^4S_{\frac{3}{2}}}(E_i,k) = \frac{e^3y_ty_sm_N}{192\sqrt{3}\pi^4}\frac{1}{E_f-E_i}\int_0^\Lambda dq'q'^2\int_0^\Lambda dq\,q^2\int_{-1}^1 d(cos\theta)\,t^{(n)\dagger}_{{}^3\mathrm{He}}(q')\,\mathcal{D}^{(n)}(E_f,q')$$
$$\times\left[\frac{O(E_i,k,q,q',\cos\theta)}{m_NE_i-k^2-q^2-kq\cos\theta}-\frac{O(E_f,k,q,q',\cos\theta)}{m_NE_f-k^2-q^2-kq\cos\theta}\right]\begin{pmatrix}-k_0 & 0 & 0\\ k_1 & 0 & 0\\ 0 & 0 & 0\end{pmatrix}. \tag{29}$$

In the above equations E_f represents the final state energy which is given by $E_f = -B_{^3\mathrm{He}}$, where $B_{^3\mathrm{He}}$ denotes the ^{3}He binding energy. The results in Eqs. (26), (29) are obtained after applying the appropriate projection operators for the initial and final states. We note that the $S^{(n)}_{4,^4S_{\frac{3}{2}}}$ must be zero since in the quartet ($S=\frac{3}{2}$) channel all spins are aligned and there is no three-body interaction in this channel because the Pauli principle forbids the three nucleons to be at the same point in space.

Finally, we stress that the $\mathcal{M}^{(n)}_x$ amplitude which is the $M1$ contribution of the $pd \to {}^3\mathrm{He}\,\gamma$ process is obtained by considering

$$\mathcal{Z}^{(n)}_t = \left(\frac{\partial}{\partial q_0}\frac{1}{D^{(n)}_t(q_0,q)}\Big|_{q_0=-\frac{\gamma_t^2}{m_N},q=0}\right)^{-1}, \tag{30}$$

as the normalization factor of the incoming deuteron wave function at N^{n}LO. We have used this normalization factor as

$$\mathcal{M}^{(n)}_x(E_i,k) = M^{(n)}_x(E_i,k)\sqrt{\mathcal{Z}^{(n)}_t}. \tag{31}$$

B. $E1$ transition

For the $E1$ matrix element of $pd \to^3$ He γ, the spin structure can be written as two orthogonal terms,

$$i(t^\dagger\sigma_a N)(\vec{\varepsilon}_d \times \vec{\varepsilon}^*{}_\gamma)_a\,, \qquad (t^\dagger N)(\vec{\varepsilon}_d\vec{\varepsilon}^*{}_\gamma). \tag{32}$$

The $E1$ transition mixes an initial P-wave state to the final S-wave helium-3. Using the $E1$ transition, the final ^{3}He ground state can be made from both initial doublet ($^2P_{\frac{1}{2}}$ and $^2P_{\frac{3}{2}}$) and quartet ($^4P_{\frac{1}{2}}$ and $^4P_{\frac{3}{2}}$) pd systems. We calculate the contribution of the diagrams in Fig. 2 as presented for the $M1$ transition. According to [20] the order of the s_5 diagram is higher than NLO, so we will not consider it in our calculation up to NLO. The $E1$ quartet amplitude for these diagrams is zero. Thus, the amplitude of the $E1$ $pd \to {}^3\mathrm{He}\,\gamma$ transition can finally be written as the sum of both initial $^2P_{\frac{1}{2}}$ and $^2P_{\frac{3}{2}}$ pd contributions by the relation

$$\mathcal{W}^{(n)}_{E1} = t^\dagger\Big[\mathcal{E}^{(n)}_{^2P_{\frac{1}{2}}}Y_{^2P_{\frac{1}{2}}} + \mathcal{E}^{(n)}_{^2P_{\frac{3}{2}}}Y_{^2P_{\frac{3}{2}}}\Big]N, \tag{33}$$

where

$$Y_{^2P_{\frac{1}{2}}} = \vec{\varepsilon}_d\vec{\varepsilon}^*{}_\gamma + i\vec{\sigma}\,\vec{\varepsilon}_d \times \vec{\varepsilon}^*{}_\gamma, \quad Y_{^2P_{\frac{3}{2}}} = 2\,\vec{\varepsilon}_d\vec{\varepsilon}^*{}_\gamma - i\vec{\sigma}\,\vec{\varepsilon}_d \times \vec{\varepsilon}^*{}_\gamma. \tag{34}$$

The $\mathcal{E}^{(n)}_y$ with $y = {}^2P_{\frac{1}{2}}, {}^2P_{\frac{3}{2}}$ for the doublet channels before multiplying the deuteron wave function normalization factor is given by

$$E^{(n)}_y(E_i,k) = \big[S^{(n)}_{0,y}(E_i,k) + S^{(n)}_y(E_i,k) + C^{(n)}_y(E_i,k)\big]u - \frac{1}{2\pi^2}\int_0^\Lambda dq\,q^2\,\big[S^{(n)}_y(E_i,q) + C^{(n)}_y(E_i,q)\big]\,\mathcal{D}^{(n)}(E_i,q)\,t^{(n,1)}_y(E_i;k,q) \tag{35}$$

with

$$S^{(n)}_y(E_i,k) = \sum_{i=1}^{4} S^{(n)}_{i,y}(E_i,k). \tag{36}$$

where the 3×3 matrix function $S^{(n)}_{i,y}$ with $i = 0,\ldots,4$ represents the contribution of the "s_i" diagram in Fig. 2 for the initial y channel at N^{n}LO ($n \leqslant 1$).

For the initial $^2P_{\frac{1}{2}}$ state, in the cluster-configuration space, we obtain

$$S^{(n)}_{0,^2P_{\frac{1}{2}}}(E_i,k) = \frac{e\,k}{3m_N}\frac{1}{E_i - E_f}\,t^{(n)\dagger}_{^3\mathrm{He}}(k)\begin{pmatrix}3 & 0 & 0\\ 0 & 1 & 0\\ 0 & 0 & 0\end{pmatrix},$$

$$S^{(n)}_{1,^2P_{\frac{1}{2}}}(E_i,k) = \frac{e\,y_t^2}{48\pi^2}\frac{1}{E_i - E_f}\,t^{(n)\dagger}_{^3\mathrm{He}}(k)\mathcal{D}^{(n)}(E_f,k)\int_0^\Lambda dq\,q^2\frac{1}{kq}\bigg[k\bigg(Q_0\bigg(\frac{m_N E_i - k^2 - q^2}{kq}\bigg) - Q_0\bigg(\frac{m_N E_f - k^2 - q^2}{kq}\bigg)\bigg)$$
$$- q\bigg(Q_1\bigg(\frac{m_N E_i - k^2 - q^2}{kq}\bigg) - Q_1\bigg(\frac{m_N E_f - k^2 - q^2}{kq}\bigg)\bigg)\bigg]\begin{pmatrix}6 & 0 & 0\\ 0 & 1 & 0\\ 0 & 0 & 4\end{pmatrix},$$

TABLE I. The experimental data and our EFT($\not\pi$) results for the cross section of the $pd \to {}^3\mathrm{He}\,\gamma$ process up to N^{n}LO ($n \leqslant 1$) are shown at energy $0.5 \leqslant E \leqslant 3$ MeV with $\Lambda = 600$. The $\sigma^{(n)}_{E1}$ and $\sigma^{(n)}_{M1}$ denote the N^{n}LO $E1$ and $M1$ cross sections, respectively. The results of the cross section are presented in units of μb.

E_{lab}(MeV)	0.5	0.7	1.0	1.4	1.8	2.5	3
$\sigma^{(0)}_{E1}$	3.5137	4.4725	5.3700	6.3061	7.2014	8.4890	9.6570
$\sigma^{(0)}_{M1}$	0.0873	0.1042	0.1283	0.1402	0.1635	0.2474	0.2511
$\sigma^{(0)}_{\mathrm{tot}}$	3.6010	4.5767	5.4983	6.4463	7.3649	8.7364	9.9081
$\sigma^{(1)}_{E1}$	2.6841	3.6494	4.5999	5.7900	6.5074	7.9707	9.0334
$\sigma^{(1)}_{M1}$	0.0898	0.1112	0.1514	0.1604	0.1803	0.2698	0.3098
$\sigma^{(1)}_{\mathrm{tot}}$	2.7739	3.7606	4.7513	5.9504	6.6877	8.2405	9.3432
σ_{exp}	2.5	3.22	4.15	5.12	5.96	7.47	8.48

$$
\begin{aligned}
S^{(n)}_{2,{}^2P_{\frac{1}{2}}}(E_i,k) &= \frac{e\,y_t^2}{24\pi^2}\frac{1}{E_i - E_f}\int_0^\Lambda dq\,q^2 t^{(n)\dagger}_{{}^3\mathrm{He}}(q)\mathcal{D}^{(n)}(E_f,q)\frac{1}{kq}\bigg[k\bigg(Q_0\bigg(\frac{m_N E_i - k^2 - q^2}{kq}\bigg) - Q_0\bigg(\frac{m_N E_f - k^2 - q^2}{kq}\bigg)\bigg)\\
&\quad - q\bigg(Q_1\bigg(\frac{m_N E_i - k^2 - q^2}{kq}\bigg) - Q_1\bigg(\frac{m_N E_f - k^2 - q^2}{kq}\bigg)\bigg)\bigg]\begin{pmatrix}0 & 0 & 3\\ 0 & 0 & -1\\ 3 & -1 & 0\end{pmatrix},\\
S^{(n)}_{3,{}^2P_{\frac{1}{2}}}(E_i,k) &= \frac{e\,y_t^2}{48\pi^2}\frac{1}{E_i - E_f}\int_0^\Lambda dq\,q^2\,t^{(n)\dagger}_{{}^3\mathrm{He}}(q)\frac{1}{k}\\
&\quad\times\bigg[\mathcal{D}^{(n)}(E_i,q)Q_1\bigg(\frac{m_N E_i - k^2 - q^2}{kq}\bigg) - \mathcal{D}^{(n)}(E_f,q)Q_1\bigg(\frac{m_N E_f - k^2 - q^2}{kq}\bigg)\bigg]\begin{pmatrix}-3 & 3 & 6\\ 3 & 1 & -2\\ 0 & 0 & 0\end{pmatrix},\\
S^{(n)}_{4,{}^2P_{\frac{1}{2}}}(E_i,k) &= 0,\\
C^{(n)}_{{}^2P_{\frac{1}{2}}}(E_i,k) &= \frac{e^3 y_t^2 m_N}{64(\pi)^4}\frac{1}{(E_i - E_f)}\int_0^\Lambda dq' q'^2\int_0^\Lambda dq\,q^2\int_{-1}^1 d(\cos\theta)\,t^{(n)\dagger}_{{}^3\mathrm{He}}(q')\,\mathcal{D}^{(n)}(E_f,q')\\
&\quad\times\bigg(q\cos\theta\bigg[\frac{O(E_i,k,q,q',\cos\theta)}{m_N E_i - k^2 - q^2 - kq\cos\theta} - \frac{O(E_f,k,q,q',\cos\theta)}{m_N E_f - k^2 - q^2 - kq\cos\theta}\bigg]\\
&\quad + \bigg(k + \frac{A}{B}q'\bigg)\bigg[\frac{O(E_i,k,q,q',\cos\theta) - O(E_f,k,q,q',\cos\theta)}{m_N E_i - k^2 - q^2 - kq\cos\theta}\bigg]\\
&\quad - q'\bigg[\frac{L(E_i,k,q,q',\cos\theta) - L(E_f,k,q,q',\cos\theta)}{m_N E_i - k^2 - q^2 - kq\cos\theta}\bigg]\bigg)\begin{pmatrix}1 & 0 & 0\\ 0 & 0 & 0\\ 0 & 0 & 0\end{pmatrix},
\end{aligned}
\tag{37}
$$

where

$$
L(E,k,q,q',\cos\theta) = \frac{1}{B\sqrt{G}}\ln\frac{y1}{y2} \tag{38}
$$

with the following parameters:

$$
y1 = (2G + D) + 2\sqrt{G}\sqrt{C + D + G},\quad y2 = (-2G + D) + 2\sqrt{G}\sqrt{C - D + G}. \tag{39}
$$

TABLE II. The cutoff variation of our EFT($\not\pi$) results for the total cross section between $\Lambda = 200$ and $\Lambda = 600$ up to N^{n}LO ($n \leqslant 1$) as a function of laboratory system energy.

E_{lab}		0.5	0.7	1.0	1.4	1.8	2.5	3.0
$Abs[1 - \frac{\sigma^{(n)}_{\mathrm{tot}}(\Lambda=200)}{\sigma^{(n)}_{\mathrm{tot}}(\Lambda=600)}]$	$n = 0$	0.0229	0.0111	0.0085	0.0071	0.0030	0.0030	0.0026
	$n = 1$	0.0040	0.0055	0.0045	0.0032	0.0033	0.0028	0.0024

Also, for the initial ${}^2P_{\frac{3}{2}}$ state the amplitudes of the $s_0,\ldots,s_4$ and c diagrams in Fig. 2 are given by

$$
\begin{aligned}
S^{(n)}_{0,{}^2P_{\frac{3}{2}}}(E_i,k) &= \frac{\sqrt{3}\,e\,k}{3m_N}\frac{1}{E_i-E_f}\,t^{(n)\dagger}_{{}^3\mathrm{He}}(k)\begin{pmatrix}3&0&0\\0&1&0\\0&0&0\end{pmatrix},\\
S^{(n)}_{1,{}^2P_{\frac{3}{2}}}(E_i,k) &= \frac{\sqrt{3}\,e\,y_t^2}{48\pi^2}\frac{1}{E_i-E_f}\,t^{(n)\dagger}_{{}^3\mathrm{He}}(k)\mathcal{D}^{(n)}(E_f,k)\int_0^\Lambda dq\,q^2\frac{1}{kq}\left[k\left(Q_0\left(\frac{m_NE_i-k^2-q^2}{kq}\right)-Q_0\left(\frac{m_NE_f-k^2-q^2}{kq}\right)\right)\right.\\
&\quad\left.-q\left(Q_1\left(\frac{m_NE_i-k^2-q^2}{kq}\right)-Q_1\left(\frac{m_NE_f-k^2-q^2}{kq}\right)\right)\right]\begin{pmatrix}6&0&0\\0&1&0\\0&0&4\end{pmatrix},\\
S^{(n)}_{2,{}^2P_{\frac{3}{2}}}(E_i,k) &= \frac{\sqrt{3}\,e\,y_t^2}{24\pi^2}\frac{1}{E_i-E_f}\int_0^\Lambda dq\,q^2t^{(n)\dagger}_{{}^3\mathrm{He}}(q)\mathcal{D}^{(n)}(E_f,q)\frac{1}{kq}\left[k\left(Q_0\left(\frac{m_NE_i-k^2-q^2}{kq}\right)-Q_0\left(\frac{m_NE_f-k^2-q^2}{kq}\right)\right)\right.\\
&\quad\left.-q\left(Q_1\left(\frac{m_NE_i-k^2-q^2}{kq}\right)-Q_1\left(\frac{m_NE_f-k^2-q^2}{kq}\right)\right)\right]\begin{pmatrix}0&0&3\\0&0&-1\\3&-1&0\end{pmatrix},\\
S^{(n)}_{3,{}^2P_{\frac{3}{2}}}(E_i,k) &= \frac{\sqrt{3}\,e\,y_t^2}{48\pi^2}\frac{1}{E_i-E_f}\int_0^\Lambda dq\,q^2\,t^{(n)\dagger}_{{}^3\mathrm{He}}(q)\frac{1}{k}\\
&\quad\times\left[\mathcal{D}^{(n)}(E_i,q)Q_1\left(\frac{m_NE_i-k^2-q^2}{kq}\right)-\mathcal{D}^{(n)}(E_f,q)Q_1\left(\frac{m_NE_f-k^2-q^2}{kq}\right)\right]\begin{pmatrix}-3&3&6\\3&1&-2\\0&0&0\end{pmatrix},\\
S^{(n)}_{4,{}^2P_{\frac{3}{2}}}(E_i,k) &= 0,\\
C^{(n)}_{{}^2P_{\frac{3}{2}}}(E_i,k) &= \frac{\sqrt{3}\,e^3y_t^2m_N}{64(\pi)^4}\frac{1}{(E_i-E_f)}\int_0^\Lambda dq'q'^2\int_0^\Lambda dq\,q^2\int_{-1}^1 d(\cos\theta)\,t^{(n)\dagger}_{{}^3\mathrm{He}}(q')\,\mathcal{D}^{(n)}(E_f,q')\\
&\quad\times\left(q\cos\theta\left[\frac{O(E_i,k,q,q',\cos\theta)}{m_NE_i-k^2-q^2-kq\cos\theta}-\frac{O(E_f,k,q,q',\cos\theta)}{m_NE_f-k^2-q^2-kq\cos\theta}\right]\right.\\
&\quad+\left(k+\frac{A}{B}q'\right)\left[\frac{O(E_i,k,q,q',\cos\theta)-O(E_f,k,q,q',\cos\theta)}{m_NE_i-k^2-q^2-kq\cos\theta}\right]\\
&\quad\left.-q'\left[\frac{L(E_i,k,q,q',\cos\theta)-L(E_f,k,q,q',\cos\theta)}{m_NE_i-k^2-q^2-kq\cos\theta}\right]\right)\begin{pmatrix}1&0&0\\0&0&0\\0&0&0\end{pmatrix}.
\end{aligned}\tag{40}
$$

As with the $M1$ transition results, the results in Eqs. (37), (40) are obtained after applying the appropriate projection operators for the initial and final states.

The $\mathcal{E}^{(n)}_y$ amplitude which is the $E1$ contribution of the $pd\to{}^3\mathrm{He}\,\gamma$ process is obtained by

$$\mathcal{E}^{(n)}_y(E_i,k)=E^{(n)}_y(E_i,k)\sqrt{\mathcal{Z}^{(n)}_t}. \tag{41}$$

V. NUMERICAL RESULTS

In order to evaluate the cross section for the $pd\to{}^3\mathrm{He}\,\gamma$ process we need the normalized ^{3}He wave function and the nucleon-dibaryon scattering amplitude. The ^{3}He wave function is obtained at LO and NLO by solving the homogenous part of Eq. (19) with applying $E=-B_{{}^3\mathrm{He}}$. For the ^{3}He wave function we use the normalization condition which is presented in Appendix A of [5]. In this process a FORTRAN code for a specific cutoff has been used. The pd scattering amplitudes at LO and NLO are obtained by solving numerically the Faddeev equations which are introduced in Sec. IV for the initial doublet and quartet channels. We solve them in a MATHEMATICA code by the Hetherington-Schick method [23–25] with a specific cutoff momentum. Using the results of the scattering amplitude and the ^{3}He wave function we solve Eqs. (24), (35) to obtain the $M1$ and $E1$ amplitudes of $pd\to{}^3\mathrm{He}\,\gamma$ process. We proceed with the numerical evaluation by using the Gaussian quadrature weights and the same cutoff momentum as before. Here, the UV divergences are handled using the three-body force $H(E,\Lambda)$ which is introduced in Eq. (3). For the leading-order three-body force $H_0(\Lambda)$ we use the equation introduced in [26], but we obtain $H_0^{\mathrm{NLO}}(\Lambda)$ for the cutoff Λ by matching the ^{3}He binding energy to the experimental value $B^{\mathrm{exp}}_{{}^3\mathrm{He}}=7.68$ MeV.

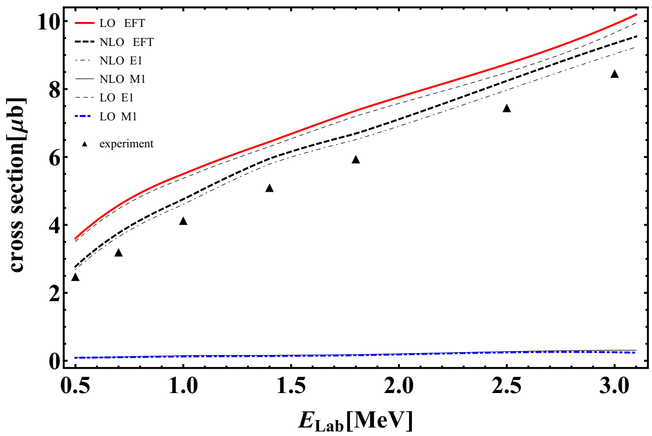

FIG. 4. Comparison between our results for $\Lambda = 600$ and experimental data. The triangular points denote the experimental data. Our results for total cross section, $E1$, and $M1$ cross section of the $pd \rightarrow {}^3\text{He}\,\gamma$ process at LO and NLO, have been shown.

As introduced in [4,5], the total N^{n}LO cross section of $pd \rightarrow {}^3\text{He}\,\gamma$ reaction is evaluated using the relation

$$\sigma_{\text{tot}}^{(n)} = \frac{(E_i - E_f)^3}{v} \times \frac{\left|\mathcal{M}^{(n)}_{{}^2S_{\frac{1}{2}}}\right|^2 + 2\left|\mathcal{M}^{(n)}_{{}^4S_{\frac{3}{2}}}\right|^2 + \left|\mathcal{E}^{(n)}_{{}^2P_{\frac{1}{2}}}\right|^2 + 2\left|\mathcal{E}^{(n)}_{{}^2P_{\frac{3}{2}}}\right|^2}{27}, \tag{42}$$

where "(n)" superscript denotes N^{n}LO results and v is the incident proton velocity in the c.m. frame.

The comparison of experimental data [27] with our EFT($\not\pi$) results for the cross section of the $pd \rightarrow {}^3\text{He}\,\gamma$ process up to N^{n}LO ($n \leqslant 1$) at energy $0.5 \leqslant E \leqslant 3$ MeV are shown in Table I. In Fig. 4 we have plotted our EFT($\not\pi$) results for total, $E1$, and $M1$ cross sections up to LO and NLO. Also, we have shown the experimental data in Fig. 4 to compare with our EFT($\not\pi$) results. We follow the power counting introduced in Ref. [5]. The EFT($\not\pi$) expansion parameter is $\frac{Q}{\bar{\Lambda}} \sim \frac{1}{3}$, where Q is the small parameter and $\bar{\Lambda}$ is the large parameter, thus the NLO diagrams enter ~33% corrections to the LO amplitude. The cross section is proportional to the square of the amplitude, so it is obvious that if for example EFT($\not\pi$) systematic error in the amplitude is "α", the systematic error in the cross section would be "2α". So, we expect a maximum error of 22% at NLO for the cross section. The NLO EFT($\not\pi$) results in Fig. 4 have the maximum error ~16.8% compared with the experimental data. This small error indicates that there is good agreement between our results and the experimental data within the range of systematic error.

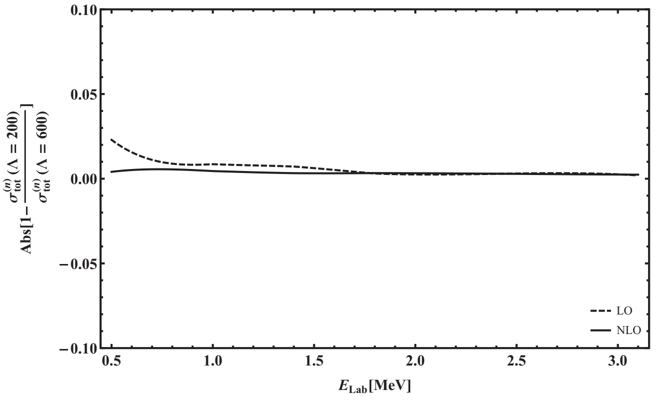

FIG. 5. Curves of cutoff variation between $\Lambda = 200$ and $\Lambda = 600$ MeV for the cross section up to N^{n}LO ($n \leqslant 1$) are plotted as a function of laboratory system energy. The dashed line and solid line correspond to our result up to LO and NLO, respectively.

In Table II we have shown the cutoff variation of our EFT($\not\pi$) results for the total cross section between $\Lambda = 200$ and $\Lambda = 600$ up to N^{n}LO ($n \leqslant 1$) at energy $0.5 \leqslant E \leqslant 3$ MeV. We have also plotted the cutoff variation of our EFT($\not\pi$) results between $\Lambda = 200$ and $\Lambda = 600$ in Fig. 5. These results indicate that the cross section of $pd \rightarrow {}^3\text{He}\,\gamma$ is cut-of independent and properly normalized.

VI. CONCLUSION AND OUTLOOK

In this paper we have calculated the cross section for $pd \rightarrow {}^3\text{He}\,\gamma$ up to NLO. We have presented our evaluation for the incoming proton with the energy $0.5 \leqslant E \leqslant 3$ MeV. The lower and upper energy limits indicate that we treat the Coulomb effect perturbatively ($E \geqslant 0.5$) MeV and the EFT($\not\pi$) breakdown scale ($E \leqslant 3$) MeV has been taken into consideration. We have considered that in the low-energy regime the $E1$ is the dominant transition and the $M1$ transition has a small but important contribution for the $pd \rightarrow {}^3\text{He}\,\gamma$ process. The experimental cross section data in this range of energy has been used in order to compare with our EFT($\not\pi$) results. The cross section results up to NLO are in good agreement with the experimental data considering the EFT($\not\pi$) theoretical uncertainties. The calculation of $pd \rightarrow {}^3\text{He}\,\gamma$ can be further applied to the calculation of parity-violating observables of the $\vec{p}d \rightarrow {}^3\text{He}\,\gamma$ reaction.

[1] E. G. Adelberger *et al.*, Rev. Mod. Phys. **70**, 1265 (1998).
[2] E. G. Adelberger, A. B. Balantekin, D. Bemmerer, C. A. Bertulani, J. W. Chen, H. Costantini, and M. Couder, R. Cyburt *et al.*, Rev. Mod. Phys. **83**, 195 (2011).
[3] G. Faldt and L. G. Larsson, J. Phys. G: Nucl. Part. Phys. **19**, 569 (1993).
[4] M. Viviani, R. Schiavilla, and A. Kievsky, Phys. Rev. C **54**, 534 (1996).
[5] M. M. Arani, H. Nematollahi, N. Mahboubi, and S. Bayegan, Phys. Rev. C **89**, 064005 (2014).
[6] H. Sadghi, S. Bayegan, and H. W. Grießhammer, Phys. Lett. B **643**, 263 (2006).
[7] F. Goeckner, W. K. Pitts, and L. D. Knutson, Phys. Rev. C **45**, R2536(R) (1992).
[8] M. K. Smith and L. D. Knutson, Phys. Rev. Lett. **82**, 4591 (1999).

[9] X. Ravndal, Nucl. Phys. A **665**, 137 (2000).
[10] H. W. Grießhammer, Nucl. Phys. A **744**, 192 (2004).
[11] S. Konig and H.-W. Hammer, Phys. Rev. C **83**, 064001 (2011).
[12] S. Konig, H. W. Grießhammer, and H.-W. Hammer, J. Phys. G: Nucl. Part. Phys. **42**, 045101 (2015).
[13] J. Vanasse, D. A. Egolf, J. Kern, S. Konig, and R. P. Springer, Phys. Rev. C **89**, 064003 (2014).
[14] D. R. Phillips, G. Rupak, and M. J. Savage, Phys. Lett. B **473**, 209 (2000).
[15] P. F. Bedaque, G. Rupak, H. W. Grießhammer, and H.-W. Hammer, Nucl. Phys. A **714**, 589 (2003).
[16] P. F. Bedaque, H.-W. Hammer, and U. van Kolck, Phys. Rev. Lett. **82**, 463 (1999); Nucl. Phys. A **646**, 444 (1999).
[17] P. F. Bedaque, H.-W. Hammer, and U. van Kolck, Nucl. Phys. A **676**, 357 (2000).
[18] G. Rupak and X. Kong, Nucl. Phys. A **717**, 73 (2003).
[19] S. Ando and M. Brise, J. Phys. G: Nucl. Part. Phys. **37**, 105108 (2010).
[20] J. W. Chen and M. J. Savage, Phys. Rev. C **60**, 065205 (1999).
[21] S. I. Ando and Ch. H. Hyun, Phys. Rev. C **72**, 014008 (2005).
[22] H. W. Grießhammer, M. R. Schindler, and R. P. Springer, Eur. Phys. J. A **48**, 7 (2012).
[23] J. H. Hetherington and L. H. Schick, Phys. Rev. **137**, B935 (1965).
[24] R. T. Cahill and I. H. Sloan, Nucl. Phys. A **165**, 161 (1971).
[25] R. Aaron and R. D. Amado, Phys. Rev. **150**, 857 (1966).
[26] D. Phillips, Czech. J. Phys. **52**, B49 (2002).
[27] ENDF/B online database at the NNDC Online Data Service, http://www.nndc.bnl.gov.